PERGAMON

International Journal of Heat and Mass Transfer 42 (1999) 1633–1644

International Journal of HEAT and MASS TRANSFER

Thermal and hydrodynamic analysis of the condensation and evaporation processes in horizontal tube desalination plant

A.D. Al-Ansari[a,*], I. Owen[b]

[a] *Mechanical Engineering Technology Department, College of Technological Studies, PO Box 19074, Khaitan 83801, Kuwait*
[b] *Department of Mechanical Engineering, The University of Liverpool, Liverpool L69 3BX, U.K.*

Received 12 April 1997; in final form 27 July 1998

Abstract

This paper considers the hydrodynamic and thermal analysis for the case where steam is condensing inside a horizontal tube while simultaneously a thin water film is evaporating on the outside of the tube. An analysis of the collective three-dimensional effects influencing the condensing and evaporating sides are presented at different operating conditions. The operating conditions include the effects of the brine mass feed rate, saturation temperatures of the condensing steam and the falling brine, and vapour flow rates. The analysis is extended to account for further effects produced by the vapour pressure and shear stresses, and also by the temperature differences between both sides of the tube. The model presented in this work consists of three regions on the condensation side and two regions on the evaporation side. The condensation side is categorized by a thin laminar condensing layer (at the top of the tube), a stratified laminary layer (at the bottom of the tube), and a laminar or turbulent vapour zone. The evaporation side has a thermally developing laminar liquid film and a thermally fully developed zone. The results of the condensation/evaporation analysis show that the dominant effects are due mainly to the brine mass feed rates, secondly to the saturation temperature differences, and least to the incoming condensing steam rates. Calculations are carried out for vapour flow of Reynolds number between 20 000 and 30 000, inlet saturation temperature of incoming steam between 60 and 70°C, and brine mass feed rate between 0.01 and 0.15 kg m^{-1} m s^{-1}.

Nomenclature

A cross-sectional area of the tube
A_v local vapour cross-sectional area
c constant used to evaluate the vapour friction factor
C_p specific heat at constant pressure of the liquid
D tube diameter
D_h hydraulic diameter of the vapour flow
f_f vapour friction factor acting at the liquid–vapour interface
f_v vapour void fraction
g gravitational constant
h_c, h_e overall heat transfer coefficients in the condensing and evaporating films, respectively
$h_{c1}(z)$ averaged local heat transfer coefficient of the condensate thin film
$h_{c2}(z)$ averaged local heat transfer coefficient of the accumulated condensate layer
$h_e(z)$ averaged local evaporation heat transfer coefficient
$h_e(\phi, z)$ local evaporation heat transfer coefficient
$h_{e1}(z)$ averaged local evaporation heat transfer coefficient in the thermally developing region
$h_{e2}(z)$ averaged local evaporation heat transfer coefficient in the fully developed region
h_{fg} latent heat of evaporation
k_c, k_e thermal conductivity of the condensing and evaporating fluids, respectively
L tube length
m constant used to obtain the vapour friction factor
$\dot{m}_f$ mass liquid feed rate of the evaporating thin film
$\dot{m}_{L1}$ mass rate entering the elemental area
$\dot{m}_{L2}$ mass rate leaving the elemental area
$\dot{m}_e$ mass rate leaving the evaporating thin liquid film and changing phase to vapour
$\dot{m}_c$ vapour mass rate entering the condensate thin liquid film and changing phase to liquid
$\dot{m}_{c1}$ mass rate of condensing thin film

* Corresponding author

0017–9310/98/$ - see front matter
PII: S0017–9310(98)00240–3

$\dot{m}_{c2}$ mass rate of vapour condensation at vapour–accumulated layer interface
dp/dy radial pressure drop
dp/dz axial pressure drop
P local vapour pressure
R tube radius
Re_v Reynolds number of the vapour
$T_{sat,c}$ vapour saturation temperature
$T_{sat,e}$ evaporating liquid film saturation temperature
T_w wall temperature
$\Delta T_c(\phi, z)$ local condensation temperature difference
$\Delta T_e(\phi, z)$ local evaporation temperature difference
U average film flow velocity
u, v, w fundamental velocity components
dV volumetric element
x, y, z fundamental coordinate system
x' variable defined by equation (A11)
y' variable defined by equation (A12).

Greek symbols
α liquid thermal diffusivity
δ_c condensating film thickness
δ_e evaporating film thickness
δ_m condensing film thickness evaluated at ϕ_s
δ_s depth of the accumulated condensate
$\delta_{s,max}$ maximum local stratified layer's depth
$\Delta\rho$ $\rho_L - \rho_v$
η variable defined as $\eta = \cos(\pi - \phi_s)$
ξ variable defined as: $\xi = \sin(\pi - \phi_s)$
μ dynamic viscosity
ν_v vapour kinematic viscosity
ρ fluid density
ρ_L density of liquid
ρ_v density of vapour
τ_{vL} shear stress of vapour on the liquid–vapour interface
ϕ_c angular measure of condensing film
ϕ_e angular measure of evaporating film
ϕ_s stratified angle of the accumulated layer
ϕ_{td} angular distance designating the beginning of evaporation at the free surface of the liquid film as shown in Fig. 3.

Other symbols
$\dot{\forall}_c$ volumetric flux of the stratified condensate layer flow
$\dot{\forall}_{c1}$ volumetric rate of the condensing thin film into the stratified layer
$\dot{\forall}_{c2}$ volumetric rate of vapour condensation onto the stratified layer
$\dot{\forall}_v$ volumetric flux of vapour flow.

1. Introduction

The desalination of sea water is a process vital to many countries in arid regions of the world. Distillation desalination plant can take different forms with the most popular being the Multi-Stage Flashing (MSF) design where the brine is heated by passing it at relatively high pressure through the inside of tubes while steam is condensing on the outside. The hot brine is then discharged into a chamber at a lower pressure so that it flashes with the vapour portion being extracted and condensed to yield fresh water. The flashing takes place in a number of stages each at a successively lower pressure. An alternative design is the Multi-Effect Boiling (MEB) evaporator where the steam is passed through the inside of the tube and the brine is evaporated on the outer surface. In the earlier designs of MEB evaporators the steam heated tubes were immersed in a pool of brine and evaporation took place by pool boiling with relatively low heat transfer rates. With this thermal constraint on the MEB system, the MSF evaporator became established as the principal type of distillation desalination plant. The MSF system has, however, a number of practical problems which lead to greater operational costs. The majority of these are related to the high pressure and temperature that the brine needs to secure a satisfactory flash and hence a worthwhile water yield. As the temperature increases, the scale formation on the inside of the tubes increases and to overcome this a rather complex cleaning process is used to clean the tube internal surfaces. For cleaning, the desalination plant is taken out of use and the tubes are flushed by passing through them a large number of balls suspended in a cleansing fluid. The cleaning system requires a continuous supply of new chemicals and balls and the subsequent disposal of the chemicals causes additional problems. There is also some tainting of the product water by the chemicals and a separate chemical purification system may be needed. Together these problems lead to greater operational costs thereby reducing the overall effectiveness of the MSF evaporators.

In response to the problems described above, the MEB system is being reassessed. The problem of low thermal performance has been overcome by using a falling film of brine over the outer surface of a vertical column of horizontal steam-heated tubes. The heat transfer rates achieved in film evaporation are considerably higher than in the forced convection heating in the MSF evaporators and this gives the MEB system a distinct advantage. Another advantage lies in the fact that unlike the MSF system, the brine does not have to be heated to such high temperatures and these can be reduced further by operating the plant under a vacuum so that typical evaporation temperatures are about 60°C thereby leading to reduced scale formation. When scale does form, it does so on the outside of the tubes which allows easier cleaning and eliminates the need for the complex cleaning plant associated with the MSF system.

To understand better the combined heat transfer processes of external evaporation and internal condensation a theoretical analysis is required which solves this con-

jugate problem whilst at the same time considering the changing hydrodynamic conditions due to flow development and mass transfer.

Falling film heat transfer has been the subject of numerous studies with some of the earliest contributions coming from Nusselt [1] who considered the formation of thin laminar films of condensate on vertical surfaces. The evaporation from the free surface of a falling film is considered in a similar way. The evaporation heat transfer coefficients of a water film flowing over an electrically heated horizontal tube was measured by Fletcher et al. [2] and this work was extended by Parken and Fletcher [3] to include different feed rates and chamber pressures. Two methods for pursuing a theoretical analysis were presented, both dependent upon laminar flow conditions which they subsequently used to explain the differences between their experimental and theoretical results. Barba and Felice [4] developed a theory to predict the evaporation heat transfer coefficient for a horizontal tube falling film without nucleate boiling. They assumed a fully developed velocity boundary layer using a turbulent model, constant film thickness and a constant initial temperature profile. They reported a respectable deviation of about $\pm 10\%$ between their calculated and experimental results. The development of the film around a horizontal tube was considered by Chyu and Bergles [5]; they defined three regions in the film: the impingement region, the thermal developing region and the fully developed region. Along with experimental data they presented two theoretical models; the first based on Nusselt's analysis and the second based on an experimentally derived correlation for fully developed film evaporation on a vertical wall. They reported better agreement with experiments for the latter theory than for the former. The flow patterns of the film as it cascaded from tube to tube was investigated by Mitrovic [6]. He noted three flow patterns as the water flow rate was increased: discrete droplets, liquid columns and liquid sheets.

Separate investigations have been made of the condensation process inside horizontal tubes. Within the general area of two-phase flow, the flow pattern inside the tube will be stratified flow as the condensate runs down the tube wall to form a layer at the bottom which will be swept along the tube by the vapour flow. This simple model will be complicated by the condensate film that forms on the pipe wall and which will cause the stratified layer to grow. Chen and Kocamustafaogullari [7] developed a physical model which accounted for the vapour flow, different interfacial shears, and pressure gradient to predict the condensation heat transfer coefficients. They assumed stratified laminar flow, a thin condensate film and neglected the surface curvature. From their numerical scheme they suggested a simplified predictive correlation for the average heat transfer coefficient. The condensation of vapour in a near-horizontal tube was considered by Moalem and Sideman [8] in both counter- and co-current flow. They assumed laminar flow, no velocity gradient and a Blasius friction factor for the vapour phase. The condensate film thickness was approximated by Nusselt's solution for a vertical wall.

The analysis of simultaneous internal condensation and external evaporation for horizontal conduits was considered by Sideman et al. [9]. They coupled the process and solved the momentum and energy equations for both. The problem was simplified by assuming no pressure drop along the tube, neglecting the inertia terms and surface tension, not considering the conduit wall thickness and assuming linear temperature profiles across the films. Their model showed an average deviation of about 55% from the available experimental data. This analysis was extended to account for variation of tube wall temperature in both the circumferential and axial directions [10]. Parabolic velocity profiles and linear temperature profiles were assumed for the films. This analysis led to an improved 30% deviation from the available experimental data.

The purpose of the present work is to build upon the work of previous researchers. A single horizontal tube will be considered; a three-dimensional physical model has been developed which allows for thermal and hydrodynamic changes around the tube and along its length. A numerical scheme has been used to solve the equations of continuity, momentum and energy for both the internal and external processes. The results obtained have been for conditions typical of those found in a desalination plant. The remainder of this paper will outline the development of the theoretical model and will illustrate its application by presenting a selection of the results obtained. For a more complete presentation of both the theoretical model and the results obtained the reader is referred to Rajab [11]. The reason for developing the model was to produce a design tool for the development of horizontal tube desalination plant. The model has been applied to a two-dimensional column of horizontal tubes to show how the variation of different operating parameters will affect the heat and mass transfer process. The present paper outlines the basics of the model, a later paper will illustrate its application.

2. Theory

2.1. Description of the model

A long metal tube with a very small wall thickness has vapour flowing inside, the vapour condenses on the tube wall as it proceeds towards the end of the tube. A subcooled liquid sheet aligned with the axis of the tube impinges upon the top of the tube and divides equally to flow around either side of it. The film re-joins at the bottom of the tube to form another sheet that impinges

again on the next tube. The enthalpy released by the condensing vapour is used to raise the temperature of the subcooled liquid to its saturation temperature and then to provide enthalpy of vaporisation for some of the liquid film to evaporate from its free surface.

2.2. Vapour condensation inside the horizontal tube

Pure vapour enters the horizontal tube and condenses on the tube wall to form two distinct layers: (i) the thin condensing layer ($0 < \phi_c \leqslant \phi_s$) and (ii) the stratified condensate layer ($\phi_s < \phi_c \leqslant \pi$). At the tube inlet the condensate layer is assumed to be annular with no accumulated portion ($\phi_s = \pi$). Further along the axial direction of the tube the accumulated layer gradually grows. The analysis of these layers assumes the following:

(1) Long tube $L \gg D$
(2) Thin film $D \gg \delta_c$
(3) Variable wall temperature $T_w = T_w(\phi_c, z)$
(4) Laminar flow of condensate layers
(5) Laminar and turbulent vapour flow.

2.2.1. Analysis of the condensing thin film layer

If we consider an element of the condensate film as shown in Fig. 1 then the mass balance yields:

$$(\dot{m}_{c2} - \dot{m}_{c1}) - \dot{m}_c = 0.$$

The net liquid mass flow $(\dot{m}_{c2} - \dot{m}_{c1})$ into and out of the element can be expressed in terms of the integrated film velocity profiles, and the vapour mass flow $(\dot{m}_c)$ condensing onto the element can be written in terms of the heat flux and the latent heat. The above mass balance therefore becomes:

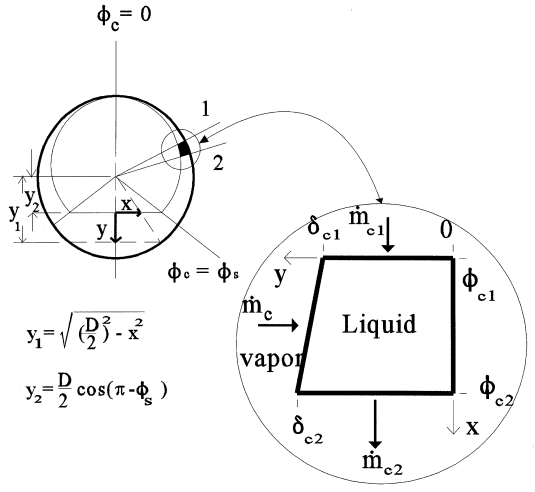

Fig. 1. Mass balance for an element of the condensate film layer.

$$\rho \frac{\delta}{\delta x} \int_{y=0}^{\delta_c} u \, dy + \rho \frac{\delta}{\delta z} \int_{y=0}^{\delta_c} w \, dy - \left[\frac{k}{h_{fg}} \frac{\partial T}{\partial y} \right]_{y=\delta_c} = 0. \quad (1)$$

The equations of motion for the element, taking into account assumptions 1 and 2, can be written as follows:

$$\mu \frac{\partial^2 u}{\partial y^2} + g \Delta\rho \sin(\phi_c) = 0 \quad (2)$$

$$\frac{\partial p}{\partial y} = 0 \quad (3)$$

$$\mu \frac{\partial^2 w}{\partial y^2} - \frac{\partial p}{\partial z} = 0 \quad (4)$$

with the following boundary conditions:

$$u = w = 0 \quad \text{at} \quad y = 0 \quad (5)$$

$$\frac{\partial u}{\partial y} = 0, \quad \mu \frac{\partial w}{\partial y} = \tau_{vL} \quad \text{at} \quad y = \delta_c. \quad (6)$$

The steady flow energy equation for the element, again taking into account assumptions (1) and (2), is written as:

$$\frac{\partial^2 T}{\partial y^2} = 0 \quad (7)$$

with the corresponding boundary conditions:

$$T = T_w \quad \text{at} \quad y = 0 \quad (8)$$

$$T = T_{sat,c}, \quad \dot{m}_c h_{fg} = -k \frac{\partial T}{\partial y} \quad \text{at} \quad y = \delta_c. \quad (9)$$

The velocity components of equation (1) can be found by solving equations (7)–(9) to produce the following equation:

$$\frac{g\rho\Delta\rho}{R\mu} \left[\delta_c^3 \sin(\phi_c) \frac{\partial \delta_c}{\partial \phi} + \frac{\delta_c^4}{3} \cos(\phi_c) \right] + \left(\frac{\rho \delta_c^2}{\mu} \right) \left[\tau_{vL} - \delta_c \frac{dp}{dz} \right] \left(\frac{\partial \delta_c}{\partial z} \right) - \left(\frac{\rho \delta_c^4}{3\mu} \right) \frac{\partial}{\partial z} \left(\frac{dp}{dz} \right) + \left(\frac{\rho \delta_c^3}{2\mu} \right) \left(\frac{\partial \tau_{vL}}{\partial z} \right) - \frac{k \Delta T_c}{h_{fg}} = 0. \quad (10)$$

Equation (10) is a non-linear partial differential equation for the film thickness, δ_c. It involves the peripheral angle, ϕ_c, the axial distance, z, and the wall temperature, $T_w(\phi, z)$. The procedure for estimating the parameters of equation (10) is described in Appendix B. The values of the film thickness are obtained numerically for given values of the other parameters by means of an iterative scheme.

2.2.2. Accumulated condensing layer analysis

The above describes how, at any point along the tube, the amount of condensate forming on the upper part $(0 \leqslant \phi_c \leqslant \phi_s)$ of the tube wall can be calculated. This condensate will then flow down the wall and will form

the accumulated layer. The accumulated layer will be swept along the tube and its thickness will increase as more condensate from the tube wall runs into it. Consider a position z (axial direction) along the tube, and consider further an elemental length of tube Δz. Figure 2 shows the mass balance on this element. Note also that the coordinate system has changed from that used for the film (see Fig. 1). The conservation principle for the control volume element of the stratified condensing layer gives:

$$\frac{m_{c,\Delta z}}{\Delta z} = \dot{m}_{c1} + \dot{m}_{c2}. \tag{11}$$

Equation (11) states that the rate of the total amount of the condensate per unit axial direction is equal to the mass rate of the condensate produced by the condensing thin film ($\dot{m}_{c1}$) plus the mass rate of condensing vapour at the vapour–accumulated layer interface ($\dot{m}_{c2}$).

The stratified accumulated layer depth (δ_s) starts at a value equal to the film thickness ($\delta_s = \delta_c$) at an angle ($\phi_c = \phi_s$) and increases to reach a maximum value at the bottom of the tube ($\delta_s = \delta_{s,max}$ at $\phi_c = \pi$). The values of $\delta_{s,max}$ are obtained geometrically by the following relation:

$$\delta_{s,max}(\pi) = \frac{D}{2}[1-\cos(\pi-\phi_s)]. \tag{12}$$

Solving for the terms of equation (11) and arranging the results in terms of volumetric rates (defined as mass flow rate divided by the product of vapour density and the tube cross-sectional area: $\dot{\forall} \equiv \dot{m}/\rho A$, commonly used to express vapour flow rather than mass flow rates), the right-hand-side terms become (detailed solutions are shown in Appendix A):

$$\dot{\forall}_{c1} = \frac{8g\Delta\rho\delta_s^3 \sin(\phi_s)}{3\pi D^2 \mu} \tag{13}$$

$$\dot{\forall}_{c2} = \frac{4h_c\Delta T_c \sin(\pi-\phi_s)}{\rho\pi D h_{fg}}. \tag{14}$$

The left-hand-side of equation (11) gives:

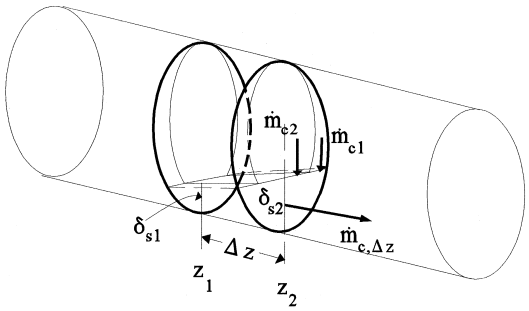

Fig. 2. Mass balance for an axial element of the accumulated condensate.

$$\dot{\forall}_c = \left(\frac{D^2}{48\pi\mu}\right)\left(-\frac{dp}{dz}\right)\left\{2\xi^3\eta - 15\xi\eta + (3+12\eta^2)(\pi-\phi_s) - \left(\frac{4\tau_{vl}}{D\left(\frac{dp}{dz}\right)}\right)[6\xi - 2\xi^3 - 6\eta(\pi-\phi_s)]\right\}. \tag{15}$$

Further details of equation (15) is found in Appendix A related to the definition of the terms and the method of the integral derivation. Also, a complete derivation for the integral [given by equation (A10)] is given by Rajab [11].

2.2.3. Analysis of the condensing vapour zone

The vapour flowing inside the horizontal tube is constantly losing part of its mass as it flows in the axial (z)-direction. The solution of the conservation of mass reveals the following rate equation (Appendix B):

$$\frac{d\dot{\forall}_v}{dz} = \frac{4h_c(z)\Delta T_c}{\rho D h_{fg}}. \tag{16}$$

Equation (16) represents the volumetric rate of vapour condensation.

2.3. Evaporation of the liquid film

Subcooled brine impinges upon the top of the tube and divides equally to flow around the tube as two identical films which then re-join to form a new liquid sheet, Fig. 3. Consider this flow in two regions: one where the flow

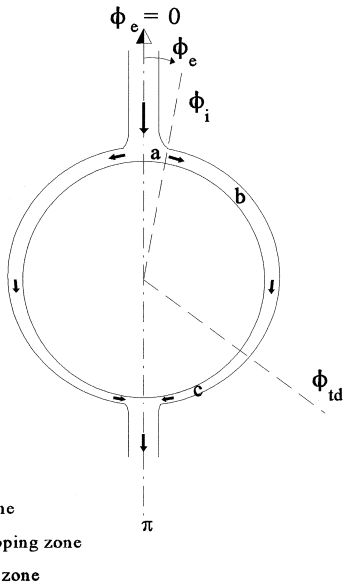

Fig. 3. Flow regions for the evaporating falling brine on a horizontal tube.

is being heated which is termed the developing region, and the other where the temperature profile is linear with the free surface at saturation temperature and evaporating (i.e. there is no boiling in the film). This second region is termed thermally developed region. The angle at which evaporation begins was shown by Chyu and Bergles [5] to be:

$$\phi_{td} = \frac{2}{\pi\alpha D}\sqrt[3]{\frac{3\mu\dot{m}_f^4}{g\rho_L^5}}. \tag{17}$$

The following assumptions are used in the analysis of the thin film:

(1) Long tube $L \gg D$
(2) Thin film $D \gg \delta_e$
(3) No pressure gradients
(4) No body forces except those due to gravity
(5) Laminar fluid flow

and the corresponding boundary conditions apply:

(1) No slip at the tube surface.

$$u = 0 \quad \text{at} \quad y = 0: \tag{18}$$

(2) No shear effects at the liquid–vapour interface:

$$\frac{\partial u}{\partial y} = 0 \quad \text{at} \quad y = \delta_e. \tag{19}$$

The tangential velocity component, u, for the developing region is assumed to be hydrodynamically developed and is obtained by solving the equation of motion with the corresponding boundary conditions. The results show:

$$u = \frac{g\Delta\rho\delta_e^2}{\mu}\sin(\phi_e)\left[\left(\frac{y}{\delta_e}\right) - \frac{1}{2}\left(\frac{y}{\delta_e}\right)^2\right]. \tag{20}$$

The mass feed, $\dot{m}_f$, is defined as

$$\dot{m}_f = \rho\bar{u}(\phi_e). \tag{21}$$

Therefore, integrating equation (21) to find the mean velocity leads to an expression for the film thickness within the thermally developing zone ($\phi_c < \phi_{td}$):

$$\delta_e = \sqrt[3]{\frac{3\mu\dot{m}_f}{g\rho\Delta\rho\sin(\phi_e)}}. \tag{22}$$

In the fully developed region, $\phi_e > \phi_{td}$, the conservation of mass applied to an element of film shows that the difference between the film mass flow entering and leaving the element is equal to the mass evaporated from its surface, i.e.:

$$\dot{m}_{L1} - \dot{m}_{L2} = \dot{m}_e. \tag{23}$$

As in the condensing film, the liquid mass flows can be found from integrating the evaporating film velocity profile, and the evaporating mass flow can be related to the heat flux:

$$\dot{m}_{L1} - \dot{m}_{L2} = \frac{\partial}{\partial x}\int_{y=0}^{\delta_e} u\,dy \tag{24}$$

$$\dot{m}_e = \left[-\frac{k}{\rho h_{fg}}\frac{\partial T}{\partial y}\right]_{y=\delta_e}. \tag{25}$$

Inserting equation (20) into equation (24), integrating at constant fluid properties then substituting this and transforming the results into cylindrical coordinates, and combining with equation (25) (under the assumption of linear temperature profile, for $\phi_e > \phi_{td}$) gives:

$$\frac{2g\rho\Delta\rho}{D\mu}\left[\delta_e^3\sin(\phi_e)\frac{\partial\delta_e}{\partial\phi} + \frac{\delta_e^4}{4}\cos(\phi_e)\right] = -\frac{k\Delta T_e}{h_{fg}}. \tag{26}$$

2.4. Combined condensation/evaporation analysis

The tube wall is assumed to be thin and to be made from a good conducting material. This means that the wall temperature is the same for both the condensing and evaporating films. An energy balance across the films shows that:

$$h_c\Delta T_c = \frac{k_c\Delta T_c}{\delta_c} = h_e\Delta T_e = \frac{k_e\Delta T_e}{\delta_e}. \tag{27}$$

The temperatures differences across the films are those between the wall temperature and the local saturation temperature, thus, assuming $k_e \approx k_c$ it is readily shown that:

$$T_w(\phi, z) = \left(\frac{\delta}{\delta_c + \delta_e}\right)T_{sat,c} + \left(\frac{\delta_c}{\delta_c + \delta_e}\right)T_{sat,e}. \tag{28}$$

The tube is discretised by dividing the fluid layers on both sides of the tube into m elements in the axial direction and n elements in the angular direction. There are $m \times n$ equal elements, and each elemental area, ΔA, is equal to the product of the axial increment, Δz, times the radial increment $\Delta\phi$. The thin film assumption implies that for the discretised element, ΔA is equal for both condensing and evaporating films. Also $\Delta\phi_c = \Delta\phi_e = \Delta\phi$, and hence, common angular notation is used for both condensing and evaporating films. At the tube inlet, $z = 0$, the condensing film thickness, $\delta_c(\phi, 0)$, is evaluated using Nusselt's solution for steam condensing on a vertical wall based on an initial guessed values for the tube wall temperature distribution, $T_w(\phi, 0)$.

Next, the evaporating film thickness for the thermally developing zone, $\delta_c(\phi, 0)$ for $\phi_e < \phi_{td}$, is calculated using equation (22) whilst the evaporating film thickness in the fully developed zone, $\delta_e(\phi, 0)$ for $\phi_e \geqslant \phi_{td}$ is calculated using equation (26). Applying the calculated film thicknesses, $\delta_c(\phi, 0)$ and $\delta_e(\phi, 0)$, into equation (28), the new wall temperature distribution is estimated. This process continues until all new values of the wall temperature distribution, $T_w(\phi, 0)$ at time $= t$, agree to within acceptable tolerance with the previously estimated values, $T_w(\phi, 0)$ at time $= t-1$.

At the next axial increment, $(\phi, \Delta z)$, the previous value

of the condensate thickness is used to calculate the stratified flow angle, ϕ_s, equation (15). New values for dp/dz and τ_{vL} are calculated and used again to re-estimate a new stratified angle; this process is repeated until the stratified angle is consistent with the pressure gradient and shear stress. The condensing flow characteristics are used to estimate local condensing film thickness, $\delta_c(\phi, \Delta z)$, described by equation (10). At the outer surface of the tube, the thermally developing angle ϕ_{td}, is determined by equation (17) and the evaporating film thickness is evaluated by equation (22), for $\phi < \phi_{td}$, and by equation (26), for $\phi \geqslant \phi_{td}$. New values for the wall temperature distribution, $T_w(\phi, \Delta z)$, is determined, equation (28), and is used to determine the condensing film thickness, $\delta_c(\phi, \Delta z)$, and the evaporating film thickness, $\delta_c(\phi_e, \Delta z)$. The computations are repeated as many times as necessary until wall temperature distribution converges to fixed values with acceptable and very small errors.

This lengthy procedure is repeated for the next axial increment $(2\Delta z, 3\Delta z, \ldots)$ until the end of the complete length $(m\Delta z)$ of the tube is covered. Local and overall heat transfer coefficients are obtained as follows:

Inside the tube

(i) in the condensing film $0 \leqslant \phi_c \leqslant \phi_s$:

$$h_{c1}(\phi_c, z) = \frac{k}{\delta_c(\phi_c, z)} \tag{29}$$

$$h_{c1}(z) = \frac{1}{\phi_s}\int_0^{\phi_s} h_{c1}(\phi, z)\,d\phi \tag{30}$$

(ii) in the stratified layer $\phi_s > \phi_c < \pi$:

$$h_{c2}(\phi_c, z) = \frac{k}{\delta_c(\phi_c, z)} \tag{31}$$

$$h_{c2}(z) = \frac{1}{\pi - \phi_s}\int_{\phi_s}^{\pi} h_{c2}(\phi, z)\,d\phi \tag{32}$$

(iii) summing these:

$$h_c(z) = \frac{\phi_s(z)}{\pi}h_{c1}(z) + \left(1 - \frac{\phi_s(z)}{\pi}\right)h_{c2}(z) \tag{33}$$

(iv) overall:

$$h_c = \frac{1}{L}\int_0^L h_c(z)\,dz. \tag{34}$$

Outside the tube

(i) $0 < \phi_e < \pi$ (for $i = 1, 2$)

$$h_{ei}(\phi_e, z) = \frac{k}{\delta_{ei}(\phi_e, z)} \tag{35}$$

$$h_e(z) = \left(\frac{\phi_{td}}{\pi}\right)h_{e1}(z) + \left(\frac{\pi - \phi_{td}}{\pi}\right)h_{e2}(z) \tag{36}$$

(ii) overall:

$$h_e = \frac{1}{L}\int_0^L h_e(z)\,dz. \tag{37}$$

3. Results

Previous investigations have been mainly concerned with values of the heat transfer coefficients of either the condensation process [7, 8] or the evaporation process [2, 3], or values for the combined processes in which many simplifying assumptions were made [9, 10]. In the present study a general solution has been produced for calculating local values of heat transfer coefficient, film thicknesses and wall temperatures allowing for different vapour flow rates and internal axial pressure gradients, mass feed rates of the brine, different saturation pressures and temperatures and different tube lengths. The results obtained from the analysis have been many and varied: only a selection, for a 3 m long 25.4 mm diameter thin-walled tube are presented herein, more detailed results are reported by Rajab [11].

In Figs 4–8 the internal (condensing) film characteristics are compared with those calculated by Chen and Kocamustafaogullari [7]. The internal pressure gradient along the tube is shown in Fig. 4, the results are presented for two different vapour flow rates and for a particular condensation saturation temperature, 100°C, and tube wall temperature at inlet, 98°C (expressed as $\Delta T_c = T_{sat,c} - T_w$). It can be seen that the present theory predicts lower values than those of Chen and Kocamustafaogullari; this is mainly because the present model uses variable wall temperatures which are found to have a significant effect. The greater negative pressure gradient predicted by the present theory is also reflected in the thinner stratified layer shown in Fig. 5. Here the results

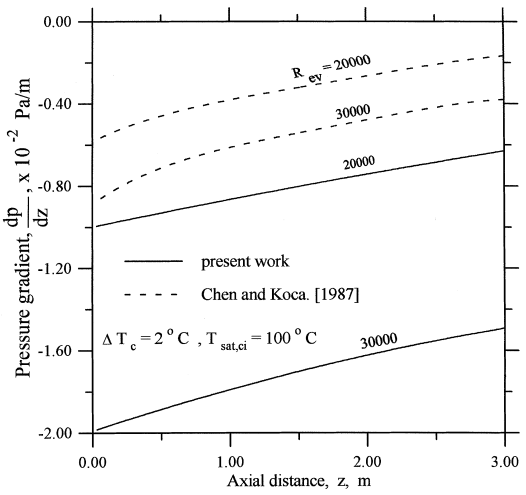

Fig. 4. Axial pressure drop at different vapour flow rates.

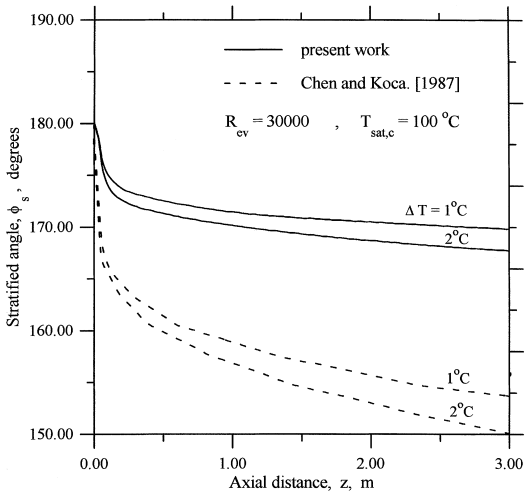

Fig. 5. Axial variation of the stratified angle for different temperature differences at higher vapour flow rates; compared to the results of Chen and Kocamustafaogullari [7].

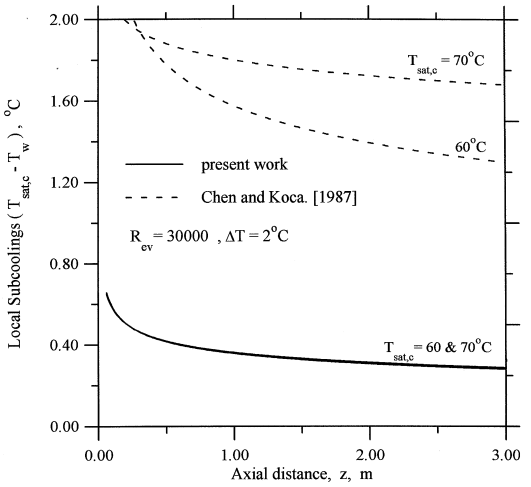

Fig. 6. Axial variation of the condensation temperature differences at different saturated temperatures.

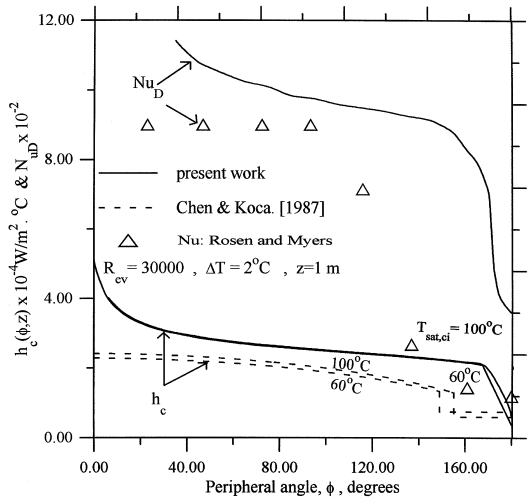

Fig. 7. Local condensation heat transfer coefficients for different saturated vapour temperatures; compared to the results obtained by Chen and Kocamustafaogullari [7] and by Rosen and Myers [12].

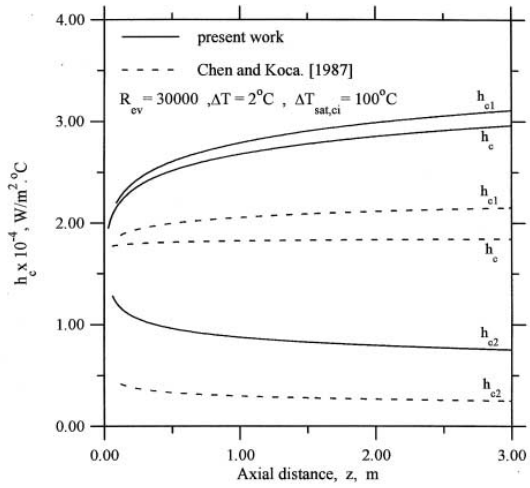

Fig. 8. Axial variations for the condensation heat transfer coefficients; comparisons with the results of Chen and Kocamustafaogullari [7].

are compared at two different tube wall inlet temperatures. In Fig. 6 the comparison between the two studies is made in terms of the temperature difference between the tube wall temperature and the saturation temperature. The data of Chen and Kocamustafaogullari is shown for two saturation temperatures, whereas for the present study only one characteristic is seen, i.e. the local subcooling differences are independent of the saturation temperature of the incoming vapour. The present study predicts lower values of local subcooling differences and this will clearly influence the heat transfer rates. In Fig. 7 there is the opportunity to compare the local heat transfer characteristics predicted by the present study with some of the limited experimental data that is available [12]. Here the circumferential distribution of the condensation heat transfer coefficient and Nusselt number can be seen. The heat transfer coefficient is seen to be independent of the saturation temperature; this is contrary to the findings of Chen and Kocamustafaogullari and is consistent with the observations made regarding Fig. 6. It can be seen that the present work predicts a higher heat transfer coefficient than that of Chen and Kocamustafaogullari and the Nusselt number predicted by the present work compares reasonably well with the

experimental data reported by Rosen and Myers [12]. The reason for the sharp fall in heat transfer rates at higher peripheral angles is the presence of the stratified layer. The calculated values for the axial distribution of heat transfer coefficient are shown in Fig. 8 for both the film portion and the accumulated layer. Again it can be seen that the present study predicts higher values. The axial heat transfer coefficient of the stratified layer, h_{c2}, decreases along the z-direction because of the continuing increase in the accumulated layer depth. The axial distribution of heat transfer coefficient for the condensing thin film layer, h_{c1}, is shown to have increasing values in the z-direction. The increasing values of the heat transfer coefficients result from the collective effects of different hydrodynamic parameters of both the condensing thin film and the vapour flow zones. The dominant parameters are the average local film thickness, and the degree of subcooling.

The condensation heat transfer coefficient and the depth of the accumulated layer calculated in the present study are compared with those obtained by Moalem and Sideman [8] in Fig. 9. The present study predicts a much thinner layer and similar, but slightly higher and varying, values for the heat transfer coefficient. These differences are due to the inclusion of the axial pressure gradient and the surface shear stress between the vapour and the layer.

Turning now to the evaporation heat transfer coefficient on the outside of the tube, the circumferential distribution of the heat transfer coefficient calculated for a particular set of conditions is shown in Fig. 10 alongside those reported by Chyu and Bergles [5]. The two predictions are seen to be identical, because the same analysis was used. In Fig. 11 the evaporation and condensation heat transfer coefficients around the circumference of the tube are both compared with the theoretical and experimental data presented by Moalem and Sideman [8]. The agreement between the present theory and the reported experiments is better than that achieved by Moalem and Sideman.

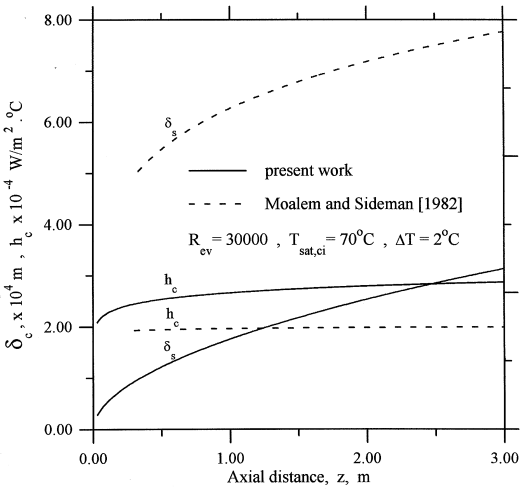

Fig. 9. Accumulated depth and condensation heat transfer coefficients vs axial distance; results compared to those obtained by Moalem and Sideman [8].

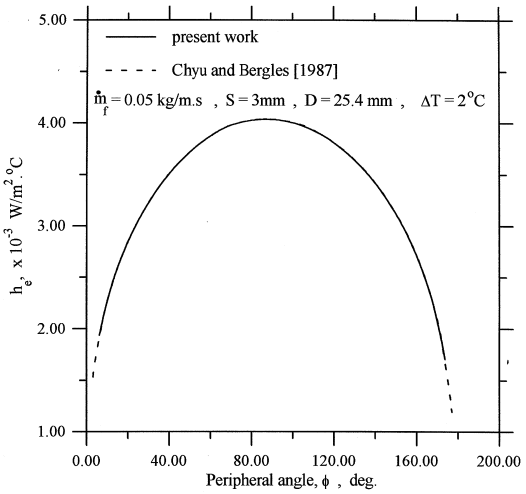

Fig. 10. Local evaporation heat transfer coefficients; compared to the results of Chyu and Bergles [5].

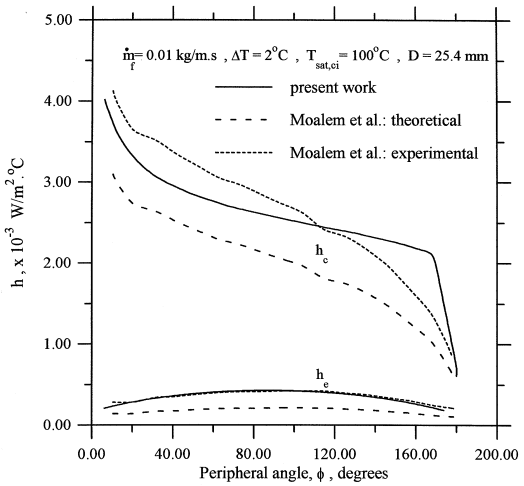

Fig. 11. Local condensation and evaporation heat transfer coefficients; the results of the present work shown with those obtained by Moalem and Sideman [10].

The present model has greater flexibility and is more complete than its predecessors, consequently it will be possible to use this as a tool in designing and developing horizontal tube falling film evaporators. As an illustration of how different variables can be investigated, Figs 12 and 13 show two effects of varying the feed rate of the brine; clearly the other main variables can also be varied and the effects of these have been investigated by

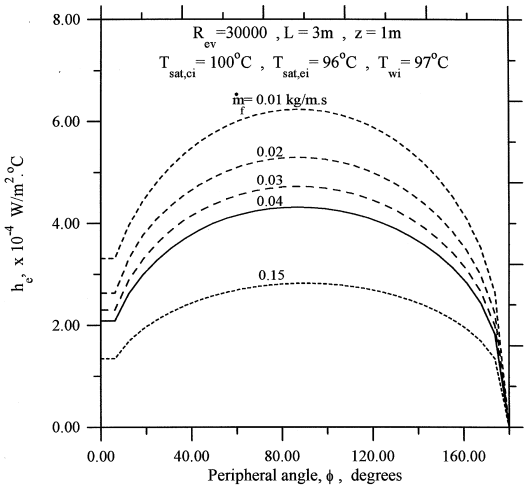

Fig. 12. Effects of brine mass feed rates on the local evaporation heat transfer coefficients.

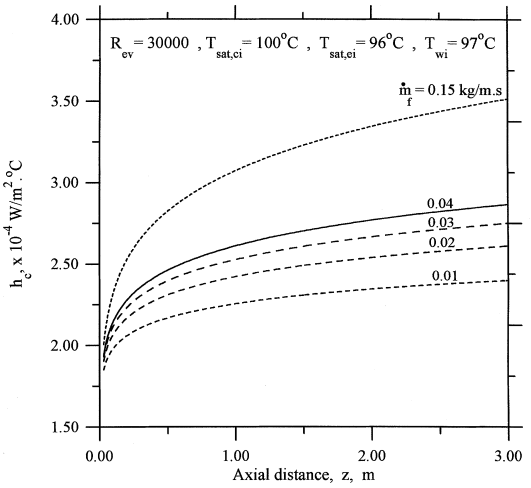

Fig. 13. Effects of brine mass feed rates on the axial condensation heat transfer coefficients.

Rajab [11]. Figure 12 shows the effect of varying the feed rate on the evaporation heat transfer coefficient around the circumference of the tube. It can be seen that as the film becomes thicker so less evaporation is achieved. Clearly to obtain maximum evaporation the film needs to be kept as thin as possible but there is a lower limit at which the film will rupture and expose a dry patch on the tube. How the mass feed rate affects the internal condensation heat transfer coefficient along the tube is shown in Fig. 13. The axial heat transfer coefficient is the sum of the amounts contributed from the condensing thin film, h_{c1}, and the local accumulated layer, h_{c2}. The portion of the heat transfer coefficients contributed from the thin film layer dominate those of the accumulated layer heat transfer coefficients. Therefore, the resulting profile for the axial condensation heat transfer coefficients follow the behaviour for the thin film heat transfer characteristics. It can be seen that as the mass feed increases so more steam has to be condensed to supply the heating. Figures 12 and 13 together indicate that if too much feed is supplied then heating steam is used to produce lots of hot water and little vapour. The results of the present study are intended to assist the system designer to have a better understanding of the effects of the thermal and hydrodynamic parameters when dealing with a more complex bundle of tubes as in a desalination plant. This work shows what would happen to the thermal and hydrodynamic performances if one or more of the parameters were varied.

4. Conclusions

The analysis presented in this paper has been developed to investigate the thermal and hydrodynamic characteristics of a horizontal tube with an internal condensing steam flow and an external evaporating thin water film. The results have been compared with the available data reported by Chen and Kocamustafaogullari [7] and by Moalem and Sideman [8] for vapour condensation inside a horizontal tube. The results of the evaporation of a thin brine film on the outside of a horizontal tube were compared with the data reported by Fletcher et al. [2] and by Parken and Fletcher [3]. The combined condensation/evaporation results were compared with the limited investigations performed by Moalem et al. [9] and by Moalem and Sideman [10]. The results of the present work show higher values for the condensation heat transfer coefficients than those reported by Sideman [13] and by Delyannis and Delyannis [14]. This was seen to be due to the use of a variable distribution for the local tube wall temperature.

Close agreement was found between the results of the present work with that of Chyu and Bergles [5] for the heat transfer coefficients of the evaporating falling thin film on a horizontal tube. In the case of combined condensation and evaporation, the predictions agree to within 5–8% of the experimental data reported by Moalem and Sideman [10] whose own theoretical predictions were not as close.

The mathematical model has been used to illustrate how various parameters affect the thermal and hydrodynamic processes. In particular, the effect of varying the brine mass feed rate and the flow rate of heating steam on the brine evaporation showed that too much brine feed simply results in a lot of hot water and little vapour. Research has continued beyond this point to show how the model can be applied to vertical columns of horizontal tubes as are found in desalination plant. This research will be reported in due course.

Appendix A: derivations for the flow equation of the stratified layer

For a long tube the axial velocity gradients are neglected and for thin film analysis the radial velocity gradient dominates the other velocity gradients. The equation of motion for the stratified layer becomes:

$$\frac{\partial^2 w}{\partial y^2} = \frac{1}{\mu}\frac{\mathrm{d}p}{\mathrm{d}z}. \tag{A1}$$

With the corresponding boundary conditions (see Fig. 1):

$$\frac{\partial w}{\partial y} = \frac{\tau_{\mathrm{vL}}}{\mu} \quad \text{at} \quad y = 0 \tag{A2}$$

$$w = 0 \quad \text{at} \quad y = \sqrt{\frac{D^2}{4} - x^2} - \frac{D}{2}\cos(\pi - \phi_{\mathrm{s}}). \tag{A3}$$

Integrating equation (A1) once and using equation (A2) to evaluate the constant of integration then integrating again and using equation (A3) to evaluate the second constant of integration yields:

$$w = \frac{1}{\mu}\frac{\mathrm{d}p}{\mathrm{d}z}\left[\frac{y^2}{2} - \frac{D^2}{8} + \frac{X^2}{2} + \frac{D}{2}\eta\sqrt{\frac{D^2}{4} - x^2} - \frac{D^2}{8}\eta^2\right] + \frac{\tau_{\mathrm{vl}}}{\mu}\left[y - \sqrt{\frac{D^2}{4} - x^2} + \frac{D}{2}\eta\right] \tag{A4}$$

where η is defined in the nomenclature.

Applying the mass conservation principle on a control volume element of the stratified layer shows:

$$\frac{m_{\mathrm{c},\Delta z}}{\Delta z} = \dot{m}_{\mathrm{c1}} + \dot{m}_{\mathrm{c2}} \tag{A5}$$

where

$$\dot{m}_{\mathrm{c1}} = 2\int_{y=0}^{\delta_{\mathrm{m}}} \rho u \,\mathrm{d}y \tag{A6}$$

$$h_{\mathrm{fg}}\,\mathrm{d}\dot{m}_{\mathrm{c2}} = h_{\mathrm{c}}(z)\,\Delta T_{\mathrm{c}}\,\mathrm{d}A. \tag{A7}$$

Equation (A6) is evaluated by substituting the tangential velocity component "u", obtained from the solution of equation (2) and the corresponding boundary conditions given by equations (5) and (6), and performing the definite integration. The following volumetric rate from the condensing thin film becomes:

$$\dot{\forall}_{\mathrm{c1}} = \frac{8g\Delta\rho\delta_{\mathrm{s}}^3\sin(\phi_{\mathrm{s}})}{3\pi D^2\mu}. \tag{A8}$$

Integrating equation (A7) for the range '$0 < \phi < \pi - \phi_{\mathrm{m}}$', the volumetric rate of condensation at the liquid–vapour free surface becomes:

$$\dot{\forall}_{\mathrm{c2}} = \frac{4h_{\mathrm{c}}(z)\Delta T_{\mathrm{c}}\sin(\pi - \phi_{\mathrm{s}})}{\rho\pi D h_{\mathrm{fg}}}. \tag{A9}$$

The left-hand-side of equation (A5) represents the rate of condensation per unit length in the axial direction and represents the area integration of the stratified flux:

$$\frac{\dot{m}_{\mathrm{c},\Delta z}}{\Delta z} = \rho\int_{x=0}^{x'}\int_{y=0}^{y'} w\,\mathrm{d}y\,\mathrm{d}x \tag{A10}$$

where

$$x' = \frac{D}{2}\xi \tag{A11}$$

$$y' = \sqrt{\frac{D^2}{4} - x^2} - \frac{D}{2}\eta \tag{A12}$$

ξ and η are defined in the Nomenclature.

Substituting equation (A4) into equation (A10) and integrating by various substitutions, the volumetric flux yields:

$$\dot{\forall}_{\mathrm{c}} = \left(\frac{D^2}{48\pi\mu}\right)\left(-\frac{\mathrm{d}p}{\mathrm{d}z}\right)\left\{2\xi^3\eta - 15\xi\eta + (3 + 12\eta^2)(\pi - \phi_{\mathrm{s}}) - \left(\frac{4\tau_{\mathrm{vl}}}{D\left(\frac{\mathrm{d}p}{\mathrm{d}z}\right)}\right)[6\xi - 2\xi^3 - 6\eta(\pi - \phi_{\mathrm{s}})]\right\}. \tag{A13}$$

Appendix B: derivations for the flow equation of the vapour zone

The mass conservation principle for the axial control volume element of the vapour zone at the liquid–vapour interface is written as:

$$h_{\mathrm{fg}}\frac{\mathrm{d}\dot{m}_{\mathrm{v}}}{\mathrm{d}z} = h_{\mathrm{c}}(z)A\,\Delta T_{\mathrm{c}} \tag{B1}$$

where 'A' is defined as the outer area of the control volume element of the vapour ($A = \pi D \times$ unit length in z-direction). Therefore, equation (B1) can be written in terms of volumetric flux as:

$$\frac{\mathrm{d}\dot{\forall}_{\mathrm{v}}}{\mathrm{d}z} = \frac{4h_{\mathrm{c}}(z)\,\Delta T_{\mathrm{c}}}{\rho D h_{\mathrm{fg}}}. \tag{B2}$$

The tangential and radial velocity components of the vapour flow are negligible compared to the axial velocity component. The equation of motion for the vapour zone is written as:

$$\frac{\rho_{\mathrm{v}}}{g_{\mathrm{c}}}w\frac{\partial w}{\partial z} = \mu\frac{\partial^2 w}{\partial z^2} - \frac{\partial p}{\partial z}. \tag{B3}$$

The axial shear stress is defined as follows:

$$\tau_{zz} = -p + 2\mu\frac{\mathrm{d}w}{\mathrm{d}z}. \tag{B4}$$

The relation between the interfacial shear stress, τ_{zz}, and the liquid–vapour shear stress, τ_{vL} is defined (by ignoring change in vapour momentum) as:

$$\frac{d\tau_{zz}}{dz} = -\frac{4\tau_{vL}}{D_h}. \tag{B5}$$

Inserting equations (B4) and (B5) in equation (B3) gives:

$$\frac{dp}{dz} = -\frac{4\tau_{vL}}{D_h} - \rho_v \dot{\forall}_v \frac{d}{dz}\left(\frac{\dot{\forall}_v}{f_v}\right) \tag{B6}$$

where

$$D_h = \frac{4A_v}{D[\phi_s + \sin(\pi - \phi_s)]} \tag{B7}$$

$$A_v = \frac{D^2}{8}(2\phi_s - \sin 2\phi_s) \tag{B8}$$

$$f_v = \frac{A_v}{A} = \frac{2\phi_s - \sin 2\phi_s}{2\pi} \tag{B9}$$

$$\tau_{vL} = \frac{f_f}{2}\rho_v w_v^2. \tag{B10}$$

In the absence of reliable friction factor for gas flow over wavy surfaces, f_f can be estimated using:

$$c = 16 \quad \text{Laminar}$$

$$f_f = c\, Re_v^{-m} \begin{cases} m = 1 \\ c = 0.046 \end{cases}$$

$$m = 0.2 \quad \text{Turbulent} \tag{B11}$$

$$w_v = \frac{\dot{\forall}_V}{f_v} \tag{B12}$$

$$Re_v = \frac{w_v D_h}{\nu_v}. \tag{B13}$$

Nusselt's solution of film condensation on vertical wall is:

$$\delta_c(\phi_c, 0) = \sqrt[4]{\frac{4\mu k D \phi_c \Delta T_c(\phi_c, 0)}{g\rho\Delta\rho h_{fg}}}. \tag{B14}$$

The procedure for estimating the condensing film thickness inside a horizontal tube is described for a control element as shown in Fig. 2 by equation (10). The analysis starts at the first element located at the inlet of the tube and the condensation film thickness is approximated by Nusselt's equation, equation (B14). The inlet pressure drop (dp/dz) and the volumetric flow rate ($\dot{\forall}_c$) is determined by the steam inlet conditions; mainly the saturated pressure and the incoming flow rate. At the inlet element is assumed that there is no stratified layer and hence the value of the stratified angle, ϕ_s, is equal to 180°.

The scheme for the remaining elements begins with the evaluation of the stratified angle, using equation (A13), based on the previous flow characteristics. Next, the flow characteristics values are re-evaluated, using equations (B4)–(B13), based on the new value of the stratified angle. This refinement scheme continues until the stratified angle converges to a fixed value. Local condensation film thickness is then determined based on the new stratified angle, using equation (10), and a backward finite difference scheme. The accumulated condensate layer thickness is bounded by an angular distance starting at $\phi_c = \phi_s$ and ending at $\phi_c = \pi$. For thin film analysis ($D \gg \delta$) the accumulated condensing layer has the following values:

$$\delta_s(\phi_c, z) = \delta_c(\phi_s, z) \quad \text{at} \quad \phi_c = \phi_s$$

$$\delta_s(\phi_c, z) = D/2[1 - \cos(\pi - \phi_s)] \quad \text{at} \quad \phi_c = \pi.$$

The accumulated depth, $\delta_s(\phi_c, z)$, increases linearly between these two values (arising from the geometry for thin film layers).

Local heat transfer coefficients, $h_c(\phi_c, z)$, are evaluated for the corresponding condensing film thickness, $\delta_s(\phi_c, z)$, equation (29). The procedure is repeated for the next element along the tube until the entire length of the tube is covered.

References

[1] W. Nusselt, Die Obreflachenkandensation des Wasser Dampfes, Z. Ver. dt. Ing., 60 (1916) 541–575.

[2] L. Fletcher, V. Sernas, W. Parken, Evaporation heat transfer coefficients for thin sea water films on horizontal tubes, Int. Eng. Chem., Process Des. Dev. 14 (4) (1975) 411–416.

[3] W. Parken, L. Fletcher, Heat transfer in thin liquid films flowing over horizontal tubes, Heat Transfer Prec. of 7th Int. Heat Trans. Conf., Munich 4 (1982) 415–420.

[4] D. Barba, R. Felice, Heat transfer in turbulent flow on a horizontal tube falling film evaporator. A theoretical approach, Desalination 51 (1984) 325–333.

[5] M. Chyu, A. Bergles, An analytical and experimental study of falling film evaporation on horizontal tube, ASME J. Heat Transfer 109 (1987) 983–990.

[6] J. Mitrovic, Influence of tube spacing and flow rate on heat transfer from a horizontal tube to a falling liquid film, 8th Int. Heat Trans. Conf., San Francisco (1986) 1949–1956.

[7] I. Chen, G. Kocamustafaogullari, Condensation heat transfer studies for stratified cocurrent two phase flow in horizontal tubes, Int. J. Heat Mass Transfer 30 (1987) 1133–1148.

[8] M. Moalem, S. Sideman, Condensation inside near horizontal tubes in co-current and counter-current flow, Int. J. Heat Mass Transfer 25 (9) (1982) 1439–1444.

[9] S. Sideman, D. Moalem, R. Semiat, Theoretical analysis of horizontal condenser–evaporator conduits of various cross-sections, Desalination 17 (1975) 167–192.

[10] D. Moalem, S. Sideman, Theoretical analysis of a horizontal condenser–evaporator tube, Int. J. Heat Mass Transfer 19 (1976) 259–270.

[11] A.D. Rajab, Heat transfer study of an immersed horizontal tube desalination system, Ph.D. thesis, The University of Liverpool, U.K., 1993.

[12] H. Rosen, J. Myers, Point values of condensation film coefficient inside a horizontal pipe, Chem. Eng. Pros. Symp. Ser. 61 (1965) 190–199.

[13] S. Sideman, Some design aspects of thin film evaporators–condensers in water desalination, In: S. Kakac, A. Bergles, ? Mayinger (Eds.), Heat Exchangers: Thermal Hydraulics, Fundamental and Design, Hemisphere, New York, 1981, pp. 681–703.

[14] A. Delyannis, E. Delyannis, Seawater and Desalting, vol. 5, Athens, 1986.